metals

MDPI

Article

Analysis of Spatter Removal by Sieving during a Powder-Bed Fusion Manufacturing Campaign in Grade 23 Titanium Alloy

Ryan Harkin, Hao Wu *, Sagar Nikam, Justin Quinn and Shaun McFadden *

Faculty of Computing, Engineering, and Built Environment, Ulster University, Derry/Londonderry BT48 7JL, UK; r.harkin1@ulster.ac.uk (R.H.); s.nikam@ulster.ac.uk (S.N.); jp.quinn@ulster.ac.uk (J.Q.)
* Correspondence: h.wu@ulster.ac.uk (H.W.); s.mcfadden2@ulster.ac.uk (S.M.)

Abstract: The Laser-based Powder Bed Fusion (L-PBF) process uses a laser beam to selectively melt powder particles deposited in a layer-wise fashion to manufacture components derived from Computer-Aided Design (CAD) information. During laser processing, material is ejected from the melt pool and is known as spatter. Spatter particles can have undesirable geometries for the L-PBF process, thereby compromising the quality of the powder for further reuse. An integral step in any powder replenishing and reuse procedure is the sieving process. The sieving process captures spatter particles within the exposed powder that have a diameter larger than a defined mesh size. This manuscript reports on Ti6Al4V (Grade 23) alloy powder that had been subjected to seven reuse iterations, focusing on the characterisation of powder particles that had been captured (i.e., removed) by the sieving processes. Characterisation included chemical composition focusing upon interstitial elements O, N and H (wt.%), particle morphology and particle size analysis. On review of the compositional analysis, the oxygen contents were 0.43 wt.% and 0.40 wt.% within the 63 µm and 50 µm sieve-captured powder, respectively. Additionally, it was found that a minimum of 79% and 63% of spatter particles were present within the captured powder removed by the 63 µm and 50 µm sieves, respectively.

Keywords: additive manufacturing (AM); Ti6Al4V; metal powder; sieving; agglomeration

Citation: Harkin, R.; Wu, H.; Nikam, S.; Quinn, J.; McFadden, S. Analysis of Spatter Removal by Sieving during a Powder-Bed Fusion Manufacturing Campaign in Grade 23 Titanium Alloy. *Metals* **2021**, *11*, 399. https://doi.org/10.3390/met11030399

Academic Editor: Elena Gordo

Received: 5 February 2021
Accepted: 24 February 2021
Published: 1 March 2021

1. Introduction

The Laser-based Powder Bed Fusion (L-PBF) process is an Additive Manufacturing (AM) technique that produces components in a layer-upon-layer manner by using a high-energy laser beam to selectively melt powder particles that had been pre-coated onto the surface of the substrate material. The relatively small spot size of the laser beam (≈0.05 to 0.1 mm) and a powder particle size typically not exceeding 70 µm, allows highly intricate components to be manufactured [1]. As a result, the L-PBF process has attracted an intense amount of interest from a wide variety of industries including aerospace, biomedical and automotive. Extra-low Interstitial (ELI) Ti6Al4V, also referred to as Grade 23, is an $\alpha + \beta$ titanium alloy that exhibits excellent corrosion resistance, biological compatibility and good strength-to-weight properties. These associated mechanical properties make Ti6Al4V one of the most popular titanium alloy used within industry.

A significant advantage associated with the L-PBF process is the ability to recycle unused powder during fabrication, for considerable cost savings benefits. Typically, only 10–50% of the powder that makes up the build volume is consolidated during component fabrication [2]. Therefore, the remaining powder is available to be reused. However, prior to the powder being reintroduced back into the production stream it must first be replenished. The quality of the reused powder is intended to remain as close to the virgin powder as possible, but this is difficult to achieve after several reuse stages [3]. Therefore, it is necessary to determine a robust powder handling procedure within an AM processing stream. A powder reuse regime will typically consist of initial powder retrieval post

fabrication, powder sieving and machine top-up. There are two types of powder reuse regimes used within industry: single-batch and top-up. A top-up reuse regime will include a powder replenishing (addition of virgin powder) stage. This rejuvenates the powder and tops-up the powder levels to meet the demand of any subsequent build. Common to both strategies is the sieving stage, where powder is typically mechanically sieved after being removed from the machine, to capture ejected material and agglomerated particles.

The L-PBF process can generate temperatures up to 10^5 °C and cooling rates between 10^6–10^8 °C/s within the melt pool [4]. It is difficult to measure the temperature profile in the melt pool, however modelling has been used to measure the thermal response within the process [5]. These processing conditions can lead to aggressive melt pool instabilities leading to the formation of spatter particles [6], ejected powder, metal vapours and condensate plumes as by-products of the focussed heating process. The transport and distribution of the by-products has been shown to be dependent on shielding gas flows and their direction relative to the build plate [7]. Spatter particles, in particular, are ejected material from the melt pool and are deposited back into the powder bed in an area local to the laser spot. Figure 1 shows an image captured during the L-PBF process. It can be seen that a few of the particles are ejected from the melt pool and blown by the inert gas flow in the build chamber. These spatter particles can fall next to the build part and form a dark discolouration within the powder bed close to the deposited part. The chemical composition and morphology of spatter particles can vary significantly from the virgin state [8]. It is observed that ejected particles can be present in 20–35% of the total area of the powder bed being processed [9]. Sutton et al. [6] have categorised spatter in relation to their particle morphology descriptions: spherical, aggregates and coarse aggregates.

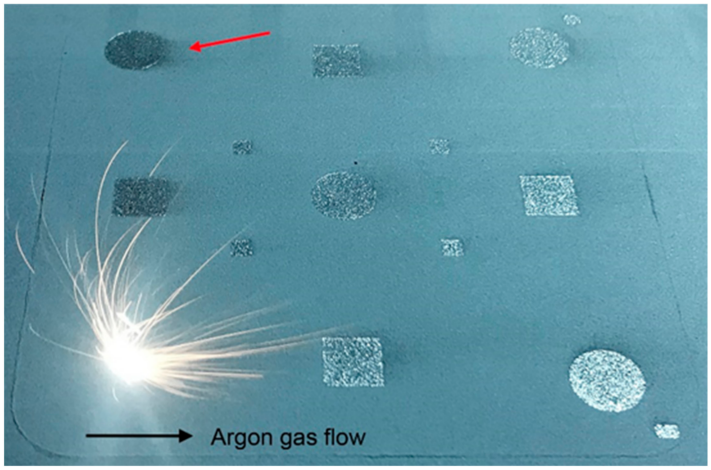

Figure 1. Image showing the ejected particles affected by the gas flow and evidence of dark discolouration due to ejected particles in the powder bed next to the deposited part (as shown by the red arrow).

There are two common forms of morphological deformation that occur: satellite and agglomeration [10]. Satellites occur whenever small particles adhere to larger particles. Whenever a melt droplet ejected from the melt pool at low angle collides with two or more powder particles surrounding the melt pool, an irregular agglomerate is formed [11]. Whenever spatter and powder particles coalesce, they form coarse agglomerated particles, that typically have a much larger size range than the original virgin powder particles (generally in the range of 25–45 μm) [12]. Agglomerated particles can have dimensions in excess of 100 μm [13].

The circularity of a batch of particle is a useful measurement and is used to indicate how the particle will spread across the platform during coating and also its tendency to flow. It has been reported that particles with a circularity greater than 0.9 are highly spherical and particles with a circularity less than 0.8 corresponding to aggregate par-

ticles [14]. The plasma atomisation technique typically produces powder particles that exhibit a high circularity and hence improved flowability. The morphological irregularity of spatter particles is therefore considered detrimental to the L-PBF process and the as-built components. The recoating blade can potentially carry large agglomerate particles across the powder bed during coating, impacting the packing density [7]. This can lead to the development of lack-of-fusion porosity, due to areas with insufficient powder coverage. An increase of ejecta (spatter particles) smaller than 30 µm was shown to increase the number of pores within as-built components [15]. Ali et al. [16] also report a surface roughness increase of 15% and 28% for components fabricated in spatter-rich zones compared with non-spatter zones.

Although the L-PBF process is performed under an inert gas atmosphere, pick-up of oxygen and other interstitial elements is unavoidable during the manufacture of ELI Ti6Al4V components [17]. The interstitial absorption of oxygen and other gaseous elements (such as nitrogen and hydrogen) leads to a change in powder composition. This is particularly evident when reusing Ti6Al4V powder [18–20]. Also, it has been shown that increased oxygen levels were present within spattered particles produced during the processing of stainless steel by the selective laser melting process [8]. If composition of certain element is sufficiently high then chemical reactions can take place, including oxide layers surrounding the particles [21]. It has been shown in L-PBF of Inconel 718 that spatter particles can have oxidation on their surfaces that was not present on the virgin particles [22]. The oxidation of spatter particles is expected to be applicable to other alloys too.

The interstitial elements in titanium alloys are known to have an effect on mechanical properties and that these compositions must be tightly controlled, especially in the ELI Grade 23 alloy. It is therefore particularly important to monitor the chemical composition of Ti6Al4V powder across a reuse regime, to ensure compliance with the ASTM F136-13 standard.

The implementation of an effective sieving process within a reuse regime is critical to the removal of deleterious spatter particles prior to rejuvenation of exposed powder by topping-up with virgin powder. Hence, sieving is consequential to the quality of the as-built component. The development of large agglomerated spatter particles and the increase of oxygen (and other elements) that can occur during processing should be minimised. A reuse regime should aim to minimise the powder property variation within the rejuvenated powder.

Aims and Objectives

The aim of this study is to analyse the effect of a two-stage sieving process during the reuse of ELI Ti6Al4V (Grade 23) powder within the L-PBF process. The powder is reused seven times and then processed through two sieves: first through a 63 µm-mesh sieve followed by a 50 µm-mesh sieve. The specific objectives include:

1. To perform chemical compositional analysis upon powder reused seven times and captured from each stage in the two-stage sieving processes, with a focus upon oxy-gen, nitrogen and hydrogen contents (wt.%);
2. To analyse particle morphology and perform quantitative shape analysis upon sieve-captured powder;
3. To assess the effectiveness of the two-stage sieving process, by comparing the results from each sieving stage with replenished (topped-up and blended) Ti6Al4V powder at the same stage as a benchmark.

2. Materials and Methods

Plasma-atomised (PA) ELI (Grade 23) Ti6Al4V powder (Carpenter Additive, Widnes, UK) was the material used throughout this study, as depicted within Figure 2. The powder characterisation results for the virgin 'as-received' powder are presented within Table 1. The particle size distribution of the powder relative to the Dv10, Dv50 and Dv90 values were: 22.3 µm, 33 µm and 48.3 µm, respectively. Component fabrication was per-

formed using an MLab Cusing R machine (GE Additive, Lichtenfels, Germany). An 80 mm × 80 mm × 90 mm build envelope was available and printing was performed upon a Ti-alloy substrate. The processing parameters used for the fabrication of the components, which remained constant throughout, were: laser power: 95 W, layer thickness: 25 µm, scanning speed: 900 mm/s, focused beam size: 0.05 mm and beam compensation: 0.5×10^{-3} s. Fabrication was performed within an argon enriched atmosphere, with the oxygen levels controlled to between 0.1–0.2% throughout.

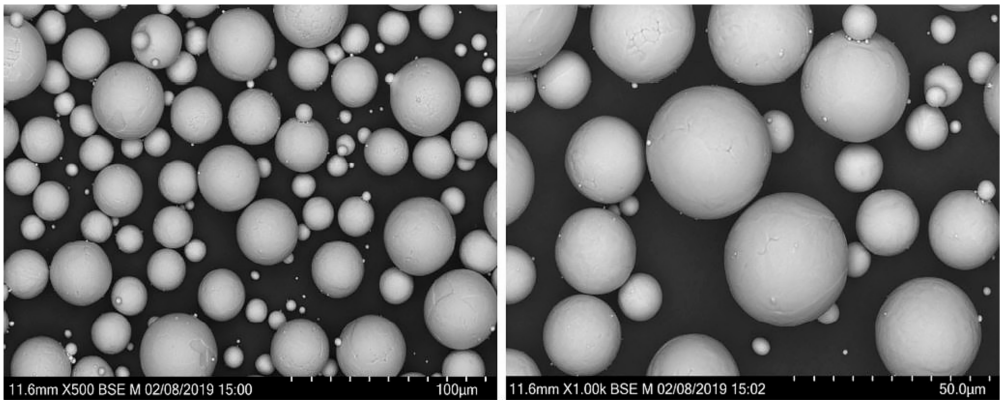

Figure 2. Scanning Electron Microscopy (SEM) images of ELI Ti6Al4V powder particles at the virgin state.

Table 1. Nominal chemical composition of Extra-low Interstitial (ELI) Ti6Al4V with compositions measured within the virgin state (wt.%).

Powder	Al	V	Fe	C	O	N	H	Ti	Other	All Other
Min	5.5	3.5	-	-	-	-	-	-	-	-
Max	6.5	4.5	0.25	0.03	0.13	0.03	0.012	Bal	0.1	0.4
Virgin	6.4	4.0	0.19	0.01	0.095	0.014	0.002	Bal	<0.1	<0.2

2.1. Reuse Strategy

Beginning from the virgin state, a top-up reuse strategy was implemented throughout. The main stages of the powder handling procedure that was performed on completion of each successful fabrication, is shown within Figure 3.

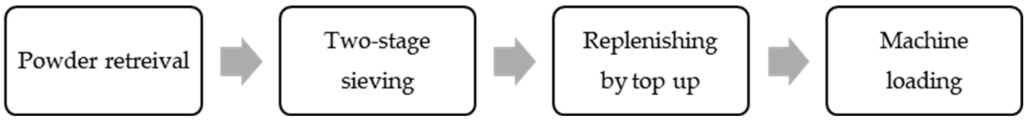

Figure 3. Powder handling procedure during a top-up recycling strategy.

2.2. Powder Sieving and Sampling Process

A two-stage powder sieving process was implemented within the powder reuse procedure, as shown within Figure 4. A mechanically vibrating Retsch AS 200 sieve (Retsch GmbH, Haan, Germany) was used, set at an amplitude of 60 Hz for 10 min. The powder was passed through a coarse 63 µm mesh followed by a fine 50 µm mesh. Those powder particles that were captured by the sieve mesh were retrieved via grab sampling for characterisation.

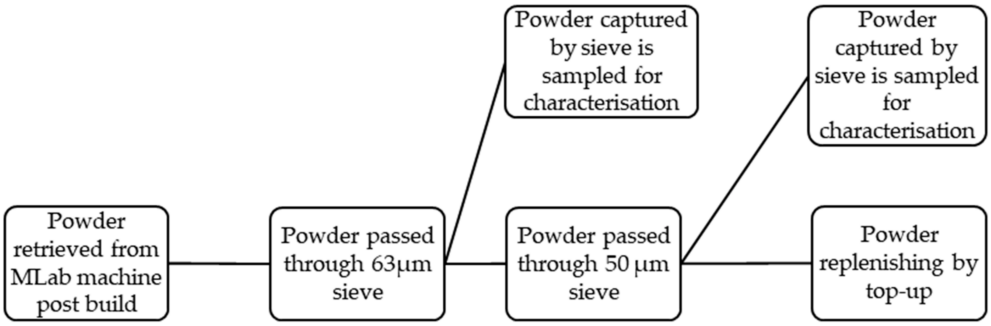

Figure 4. The powder sieving procedure implemented on completion of each build, including the powder sampling points.

2.3. Sample Preparation

The titanium powder was prepared for metallographic analysis, to identify agglomerate or splatter particles and to investigate the morphology at each stage of the sieving process. Initially, 5 g powder sample was hot mounted in Bakelite compound. The samples were ground (water-assisted grinding) using SiC papers from P1200 up to P4000, then polished using 3 µm diamond suspension and finally 0.06 µm colloidal silica suspension.

2.4. Material Characterisation

2.4.1. Chemical Composition

The captured powder was characterised for chemical compositional analysis by Inert Gas Fusion (IGF, LECO, St. Joseph, MI, USA) in accordance with the ISO 17025, focusing upon oxygen, nitrogen and hydrogen content (wt.%). Seven-times recycled powder was characterised at the two-step sieving stages (63 µm and 50 µm sieves). Afterwards a sample was taken from the replenished powder (topped up and blended) for interstitial composition analysis.

2.4.2. Bulk Morphology

Micrographs were acquired using a Leica DMi8 optical microscope (Leica Microsystems, Wetzlar, Germany), producing bright field images of the processed powder particles. Qualitative analysis of the micrographs was performed to identify the presence of spatter particles after each sieving stage. SEM (Hitachi High-Tech, Tokyo, Japan) was used to determine the morphology of the sieved powder particles.

2.4.3. Powder Morphology

Quantitative analysis was performed upon the micrographs of the titanium alloy powder using automatic thresholding, using the software ImageJ. The circularity (C) of each particle was calculated within ImageJ using Equation (1), where A is the area of the particle and P is the perimeter of the particle. The particle's area also allowed for calculation of an approximate diameter of each particle to be derived.

$$C = \frac{4\pi A}{P^2}. \quad (1)$$

2.4.4. Classification of Spatter Particles

Each powder particle was classified in relation to their circularity and diameter, as shown in Table 2. Volume and weighted number distribution of virgin ELI Ti6Al4V powder was originally determined using the Laser Size Diffraction (LSD, Malvern Panalytical, Worcestershire, UK) technique, in accordance with the ASTM B822 standard. The maximum particle diameter reported from the LSD analysis was 76 µm and therefore this diameter will be used as benchmark data for this study. Additionally, it was considered that particles with a circularity less than 0.8 were a form of spatter. Four types of spatter particles

were defined within this study, with Type 5 referring to the typical particle size range of PA powder.

Table 2. Classification of agglomeration particles relative to the particle circularity (*C*) and particle diameter (*D*).

Particle Type	Particle Geometry	Classification
Type 1	$D > 76$ µm and $C < 0.8$	Coarse agglomerate
Type 2	$D > 76$ µm and $C > 0.8$	Spherical agglomerate
Type 3	$D < 76$ µm and $C < 0.8$ ONLY	Aggregate
Type 4	$D < 14.5$ µm	Fine particulates
Type 5	14.5 µm $< D <$ 76 µm and $C > 0.8$	Plasma-atomised particle

3. Results

3.1. Chemical Compositional Analysis

The results of the oxygen content (wt.%) within the ELI Ti6Al4V powder at various stages throughout the sieving process are presented within Figure 5. The error bars represent measurement uncertainty. The measured oxygen content within the 63 µm sieve-captured and 50 µm sieve-captured powder was 0.43 wt.% and 0.40 wt.%, respectively. Both these values exceed the maximum threshold for both the ELI grade (Grade 23) of 0.13 wt.% and Grade 5 of 0.2 wt.% (ASTM F136-13). However, the oxygen content within the sieved (0.131 wt.%) and blended powder (0.127 wt.%) complied with the ELI Ti6Al4V requirements.

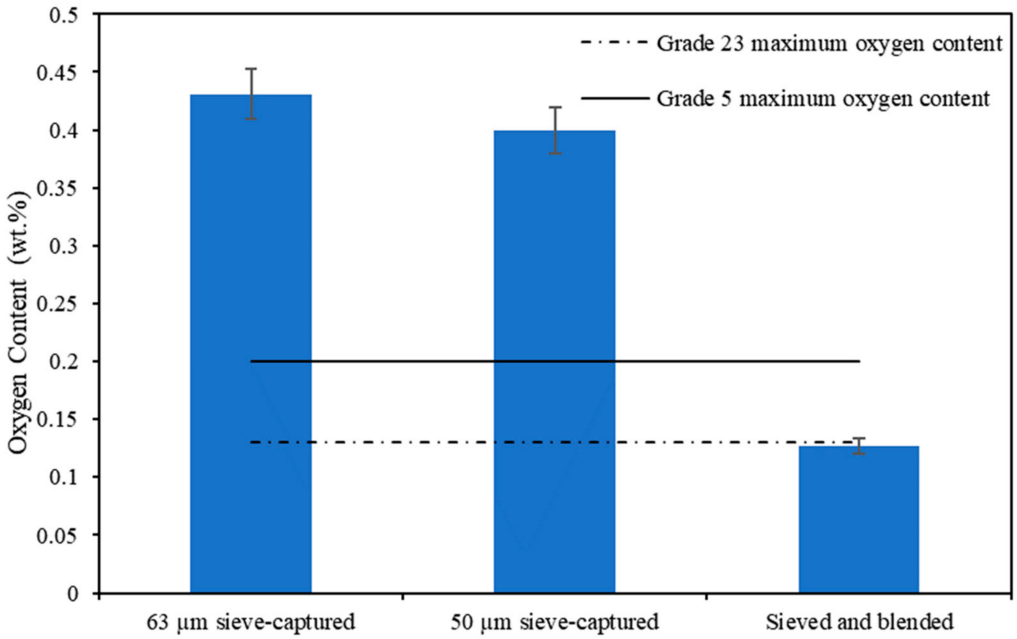

Figure 5. Oxygen analysis within the powder samples comparing 63 µm sieve-captured, 50 µm sieve-captured and post sieved powder at seven recycle iterations. Error bars represent the systematic uncertainty.

The results of the nitrogen and hydrogen content (wt.%) within the Ti6Al4V powder at each stage of the sieving process are presented within Figure 6. The error bars, where shown, represent measurement uncertainty. The nitrogen content significantly exceeded the maximum threshold of the ELI Ti6Al4V grade (0.03 wt.%) within both sieve-captured states. The nitrogen content was 0.234 wt.% and 0.230 wt.% within the 63 µm sieve-captured and 50 µm sieve-captured powders, respectively. The chemical composition of the ELI Ti6Al4V powder however complied with the ASTM F136-13 standard post sieving and blending.

The hydrogen content was returned to lower than the ELI Ti6Al4V limit of 0.012 wt.% after the 50 µm sieving stage. Hydrogen content was comfortably lower than the required range for the sieved and blended (topped-up) powder.

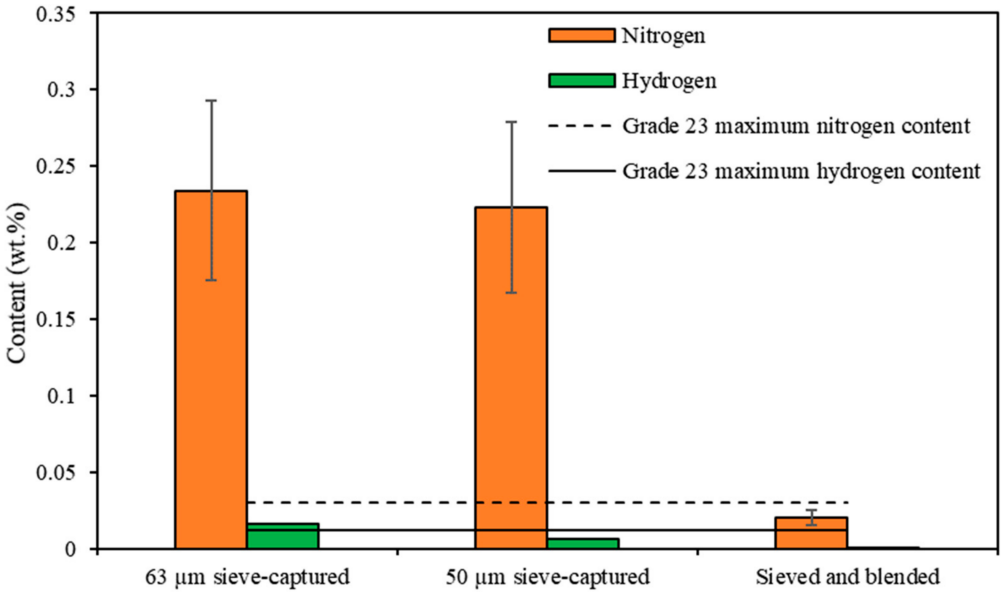

Figure 6. Nitrogen and hydrogen analysis within the powder samples comparing 63 µm, 50 µm sieve-captured and post sieved powder at seven recycle iterations. Error bars represent the systematic uncertainty.

3.2. Bulk Morphology – Sieve-Captured Powder

Powder particle surface features and morphology were initially qualitatively captured by an optical microscope, as shown within Figure 7. Two-dimensional (2D) surface micrographs allowed the presence of spatter and non-spatter particles to be initially identified within the sieve-captured powder.

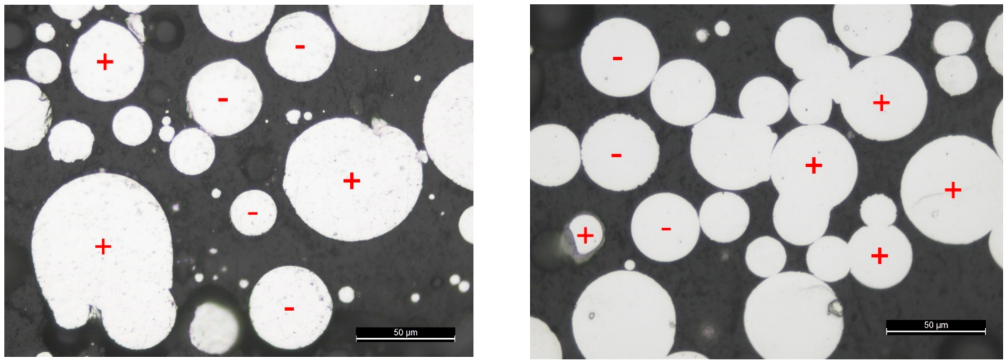

(**a**) (**b**)

Figure 7. Two-dimensional (2D) morphological analysis of Ti6Al4V powder for the identification of spatter particles, within (**a**) 63 µm sieve-captured powder and (**b**) 50 µm sieve-captured powder. The plus symbol (+) represents spatter particles and the minus (−) symbol represents the desired particle geometry for Laser-based Powder Bed Fusion (L-PBF) process (Type 5).

3.3. Bulk Morphology—Recycled Powder

SEM images of powder samples post sieving and replenishing after seven reuses is shown in Figure 8. The majority of the powder particles appear to be highly spherical with some indication of partially sintered, broken and satellited particles (shown by the arrows).

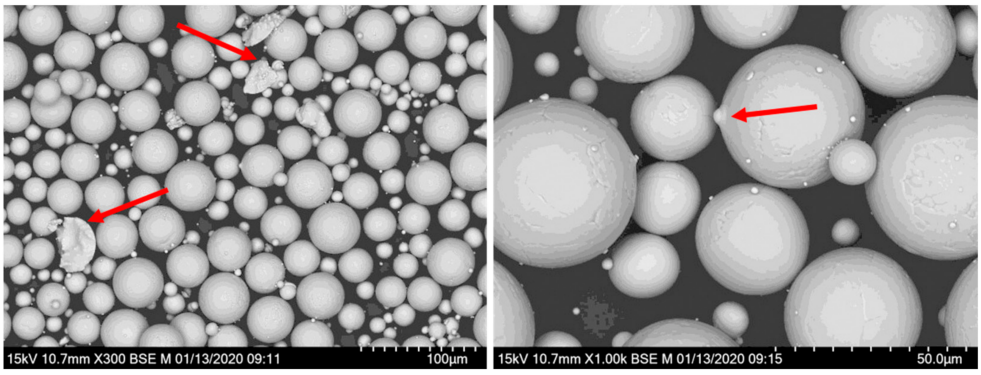

Figure 8. SEM images of powder samples after sieving and blending.

3.4. Particle Shape Analysis

Particle shape analysis was used to qualitatively analyse the frequency of each type of particle within the sieve-captured powder sample, presented in Figure 9. The frequencies of spatter particles (summation of all Type 1 to Type 4) present within the 63 µm sieve-captured and 50 µm sieve-captured were 79.10% and 63.32%, respectively. It should be noted that 63 µm sieve was effective, perhaps counterintuitively, in removing the majority of the particulate particles perceived to be below 14.5 µm. Given the clear evidence of the existence of satelliting particles these could be smaller particles attached to larger particles that had been revealed by the sectioning process.

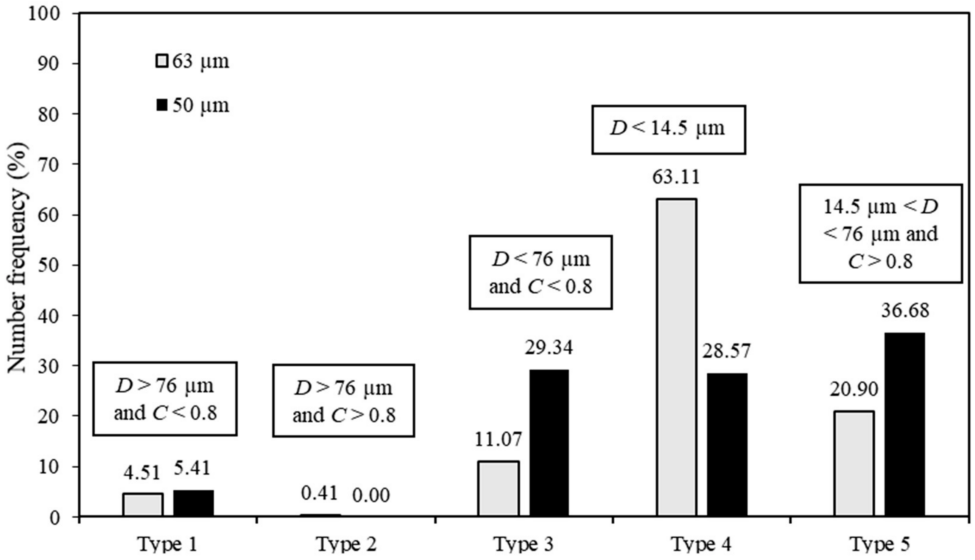

Figure 9. The number frequency of each type of powder particle present within the 63 µm and 50 µm sieve-captured Ti6Al4V powder.

4. Discussion

On review of the results presented within this study, it is clear that a variety of spatter types had been formed during processing. Also, the powder properties of these spatter particles had deviated significantly from its virgin state, particularly in relation to the chemical composition, morphology and shape. On examination of the compositional analysis within seven times recycled powder, the oxygen and nitrogen content (wt.%) had significantly exceeded the maximum acceptable levels in the sieve-captured state. The oxygen content in both 63 µm and 50 µm sieve-captured states were between 0.4 wt.% and 0.45 wt.%, which is more than three times the 0.13 wt.% limit of Grade 23 Ti6Al4V. The nitrogen levels were 0.234 wt.% and 0.230 wt.% for the 63 µm and 50 µm sieve-captured samples, respectively. These nitrogen content levels are an order of magnitude greater than

the Grade 23 acceptable limit (0.03 wt.%). However, after sieving and topping up both oxygen and nitrogen returned to levels acceptable for the Grade 23. Hydrogen returned below the maximum limit (0.012 wt.%) at the 50 µm sieve-captured powder state, which would suggest that the first sieving stage was sufficient to remove particles with high hydrogen content.

The results from the study were taken from a broader top-up study [3]. This was cycle number 7 from a nine-cycle powder reuse regime. Within the broader context across the reuse regime, the oxygen content within the ELI Ti6Al4V powder increased above the maximum limit of the Grade 23 alloy. The regression analysis presented in reference [3] gave a linear slope of 0.004 (wt.% per cycle) with a p-value of 7.84×10^{-8}. Since this p-value is less than 0.05, the trend in the oxygen increase over all nine cycles was significant. This investigation shows oxygen content is reduced by sieving, but eventually oxygen accumulates over several reuse cycles. The same analysis as reported in reference [3] showed no significant trend in nitrogen or hydrogen pickup over several cycles, therefore the sieving process shown here is essential in removing oxygen and nitrogen at each stage.

On comparison of the compositional analysis of sieve-captured and sieved and blended powder samples, it is clear that the spatter particles contain increased interstitial (O, N and H) levels. Similar findings were reported for a different alloy reported by Sutton et al., where the oxygen content of heat affected (spatter) 304 L stainless steel powder was three times greater than the virgin state [6]. Despite processing within a controlled environment, as in this case purged with argon, it is impossible to completely eliminate interstitial elements from the L-PBF build chamber. Oxygen pick-up of molten titanium is therefore inevitable during processing. Instead of forming oxide layers, it has been suggested that oxygen completely dissolves within titanium solid solution when at a low composition [23]. Hence, it was critical to characterise titanium spatter particles using the IGF technique.

The maximum, minimum and mean diameter of the coarse agglomerate particles (Type 1) present within the sieve-captured powder conditions, derived by 2D analysis, are shown within Table 3. The maximum diameter of agglomerate reported was 155.58 µm which was more than three times larger than the desired upper particle size range (45 µm) for powder used within the L-PBF process. Similar spatter sizes have reported in previous studies [24,25]. Due to the geometry of the coarse agglomerate and spherical agglomerate (Type 2) particles stated within this study ($D > 76$ µm), it is likely that the majority of these particles will be captured during sieving. Within this study, the circularity of the particles was assumed as 1 to derive a theoretical diameter from the area of each particle.

Table 3. Analysis of coarse agglomerate (Type 1) particle geometry in relation to the maximum, minimum and mean diameter.

Type 1	**63 µm Sieve-Captured Powder**			**50 µm Sieve-Captured Powder**		
	Max	Min	Mean ± STD	Max	Min	Mean ± STD
Diameter, D (µm)	155.58	79.81	100.78 ± 26.48	128.69	79.81	96.30 ± 14.30

Figure 10 displays a micro-graph of a coarse agglomerate particle, measured relative to the particle height (P_h) and particle width (P_w). This shows the presence of particles which has major dimensions greater than the sieve size. The agglomerate shown had a P_h value of 80.32 µm and a P_w value of 62.23 µm. The P_w value of the particle allowed the particle to pass through the 63 µm mesh, but not through the 50 µm mesh. Hence, it is possible that some agglomerated particles may still be present within the powder after sieving. Additionally, it was shown that spatter particles can have a particle size similar to the size distribution of plasma atomised powder (Types 3, 4 and 5). Within the 50 µm sieve-captured powder, 13.13% of spatter powder particles present ranged between 25–45 µm. It has been reported elsewhere that 85% of spatter particles can have a size distribution range similar to virgin powder [26]. Therefore, due to the mesh sizes it is likely

that spatter particles will remain present within the reused powder post sieving but at a low percentage.

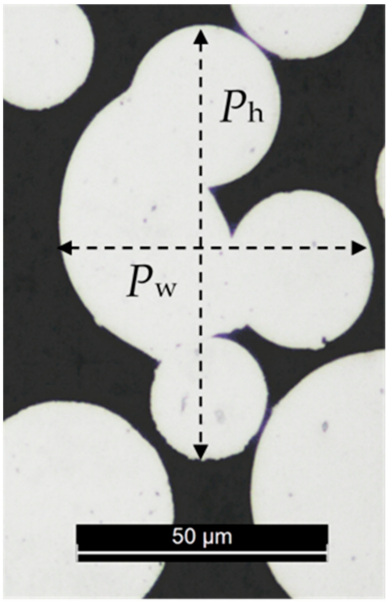

Figure 10. Coarse agglomerate particle captured by the 50 µm mesh.

In addition to geometry, the Ti6Al4V powder particles were classified in accordance with their circularity. The mean circularity of the 63 µm sieve-captured and 50 µm sieve-captured powder particles was 0.87 ± 0.19 and 0.73 ± 0.25, respectively. As a result of an increased frequency of spatter particles within the sieve-captured powder, a lower powder circularity was reported. Post sieving, the titanium powder had a mean circularity value of 0.97 ± 0.07, indicating that the two-stage sieving process was effective in minimising the amount of spatter particles. As non-spherical powder particles can negatively affect both the powder flowability and packing density within the L-PBF process, it is important to minimise the presence of such unwanted particles [27].

The production of highly spherical titanium powder for AM processes is considered expensive. Therefore, the ability to replenish and reintroduce unused, exposed powder within the L-PBF process leads to substantial cost saving. A term commonly used across the manufacturing industry is the 'buy-to-fly ratio'. Defined as the ratio of the weight of the raw material used to manufacture a component to the actual weight of the final component. In addition to the near-net shape manufacturing capabilities, the inclusion of the powder removed through sieving within a reuse regime for L-PBF process should be considered within the buy-to-fly ratio calculations.

As shown by Figure 7, the majority of powder particles captured by the sieve are spatter. These particles had an undesired geometry or circularity for the L-PBF process. Therefore, the sieving process is a critical stage of a powder reuse process for eliminating or reducing such particles. Not only does the recycling minimise the powder property deviation from the virgin state, but also a minimal amount of powder is lost during sieving. Within this study, a mean powder percentage loss of 2.62 ± 2.21 wt.% occurred across the current top-up reuse regime as reported elsewhere [3]. Provided a sufficient quantity of powder, post reuse, is available to complete the subsequent AM build, the two-stage sieving process used within a top-up reuse process is effective for rejuvenating the exposed powder.

5. Conclusions

Chemical compositional analysis was performed upon sieve-captured and sieved ELI Ti6Al4V powder via the IGF technique, that had been exposed to a seven-iteration top-up reuse regime. The oxygen content within the 63 µm sieve-captured and 50 µm sieve-

captured powder was 0.43 wt.% and 0.40 wt.%, respectively. Both powder states, exceeded the maximum thresholds for both the Grade 23 and Grade 5 Ti6Al4V. The nitrogen content also significantly exceeded the maximum threshold of Grade 23 within both sieve-captured states. However, post sieving and blending the oxygen and nitrogen content returned to below the maximum thresholds of Grade 23. Hydrogen returned to an acceptable level within the 50 µm sieve-captured powder state.

The bulk morphology of the sieve-captured powder was initially qualitatively observed via surface micrographs to identify the presence of spatter particles. On review, agglomerated powder particles were clearly identifiable from non-spatter particles. The powder morphology of the sieved and blended powder was analysed by SEM imaging. As expected with processed PA powder, highly spherical particles were observed with some evidence of satelliting, partially sintered and broken powder particles.

Quantitative shape analysis was performed upon the surface micrographs of the Ti6Al4V powder to determine the frequency of each particle form present within sieve-captured powder. The particle diameters and actual circularity values were measurements used to characterise the particles (see Table 2). It was calculated that the frequency of spatter present within the 63 µm and 50 µm sieve-captured was 79.10% and 63.32%, respectively. The largest form of spatter reported was a coarse agglomerate (Type 1) particle, that had a diameter of 155.58 µm. Due to the geometry of coarse and spherical agglomerate (Type 2) particles stated within this study ($D > 76$ µm), it was concluded that the majority of these particles would be captured during sieving. Also, the mean circularity of the 63 µm sieve-captured and 50 µm sieve-captured powder particles was 0.87 ± 0.19 and 0.73 ± 0.25, respectively. The powder had a mean circularity value of 0.97 ± 0.0 after sieving and blending, indicating a reduction of spatter particles presents within the reusable ELI Grade 23 Ti6Al4V powder. However, it was shown that a coarse agglomerate particle with height (P_h) and particle width (P_w) less than the mesh size did pass through the sieve, resulting an increasing level of oxygen content.

Plasma-atomised titanium powder is considered expensive, therefore the financial feasibility of including a reuse regime was evaluated by quantifying powder loss during sieving. Across a seven-iteration top-up reuse regime, a mean powder percentage loss of 2.62 ± 2.21 wt.% occurred. A minimal amount of powder was lost during sieving and, of the particles captured, the majority were spatter with a non-desirable morphology and chemical composition for the L-PBF process. Therefore, this study has shown that an effective two-stage powder sieving regime was implemented to maintain the quality of the feedstock material. Financial benefits from an effective reuse strategy are apparent but powder removed through sieving should be considered when calculating the buy-to-fly ratio.

Author Contributions: Conceptualization, R.H.; data curation, R.H., H.W. and S.N.; formal analysis, R.H.; funding acquisition, J.Q. and S.M.; investigation, R.H., H.W. and S.N.; methodology, R.H., H.W. and S.N.; supervision, J.Q. and S.M.; visualization, R.H. and H.W.; writing—original draft, R.H.; writing—review & editing, R.H., H.W., S.N., J.Q., and S.M. All authors have read and agreed to the published version of the manuscript.

Funding: This research was funded by INTERREG VA Programme, managed by the Special EU Programmes Body (SEUPB), as part of the NW CAM project. The APC was funded through the NW CAM project.

Acknowledgments: The North West Centre for Advanced Manufacturing (NW CAM) project is supported by the European Union's INTERREG VA Programme, managed by the Special EU Programmes Body (SEUPB). The views and opinions in this document do not necessarily reflect those of the European Commission or the Special EU Programmes Body (SEUPB). If you would like further information about NW CAM please contact the lead partner, Catalyst, for details.

Conflicts of Interest: The authors declare no conflict of interest.

References

1. Sutton, A.T.; Kriewall, C.S.; Leu, M.C.; Newkirk, J.W. Powder characterisation techniques and effects of powder characteristics on part properties in powder-bed fusion processes. *Virtual Phys. Prototyp.* **2017**, *12*, 3–29. [CrossRef]
2. Santecchia, E.; Spigarelli, S.; Cabibbo, M. Material Reuse in Laser Powder Bed Fusion: Side Effects of the Laser—Metal Powder Interaction. *Metals* **2020**, *10*, 341. [CrossRef]
3. Harkin, R.; Wu, H.; Nikam, S.; Quinn, J.; McFadden, S. Reuse of Grade 23 Ti6Al4V Powder during the Laser-Based Powder Bed Fusion Process. *Metals* **2020**, *10*, 1700. [CrossRef]
4. Liu, Y.; Yang, Y.; Mai, S.; Wang, D.; Song, C. Investigation into spatter behavior during selective laser melting of AISI 316L stainless steel powder. *Mater. Des.* **2015**, *87*, 797–806. [CrossRef]
5. Ahsan, F.; Ladani, L. Temperature Profile, Bead Geometry, and Elemental Evaporation in Laser Powder Bed Fusion Additive Manufacturing Process. *JOM* **2019**, *72*, 429–439. [CrossRef]
6. Sutton, A.T.; Kriewall, C.S.; Leu, M.C.; Newkirk, J.W.; Brown, B. Characterization of laser spatter and condensate generated during the selective laser melting of 304L stainless steel powder. *Addit. Manuf.* **2020**, *31*, 100904. [CrossRef]
7. Ladewig, A.; Schlick, G.; Fisser, M.; Schulze, V.; Glatzel, U. Influence of the shielding gas flow on the removal of process by-products in the selective laser melting process. *Addit. Manuf.* **2016**, *10*, 1–9. [CrossRef]
8. Obeidi, M.A.; Mussatto, A.; Groarke, R.; Vijayaraghavan, R.K.; Conway, A.; Kaschel, F.R.; McCarthy, E.; Clarkin, O.; O'Connor, R.; Brabazon, D. Comprehensive assessment of spatter material generated during selective laser melting of stainless steel. *Mater. Today Commun.* **2020**, *25*, 101294. [CrossRef]
9. Criales, L.E.; Arısoy, Y.M.; Lane, B.; Moylan, S.; Donmez, A.; Özel, T. Laser powder bed fusion of nickel alloy 625: Experimental investigations of effects of process parameters on melt pool size and shape with spatter analysis. *Int. J. Mach. Tools Manuf.* **2017**, *121*, 22–36. [CrossRef]
10. Powell, D.; Rennie, A.E.; Geekie, L.; Burns, N. Understanding powder degradation in metal additive manufacturing to allow the upcycling of recycled powders. *J. Clean. Prod.* **2020**, *268*, 122077. [CrossRef]
11. Terrassa, K.L.; Haley, J.C.; Macdonald, B.E.; Schoenung, J.M. Reuse of powder feedstock for directed energy deposition. *Powder Technol.* **2018**, *338*, 819–829. [CrossRef]
12. Vock, S.; Klöden, B.; Kirchner, A.; Weißgärber, T.; Kieback, B. Powders for powder bed fusion: A review. *Prog. Addit. Manuf.* **2019**, *4*, 383–397. [CrossRef]
13. Young, Z.A.; Guo, Q.; Parab, N.D.; Zhao, C.; Qu, M.; Escano, L.I.; Fezzaa, K.; Everhart, W.; Sun, T.; Chen, L. Types of spatter and their features and formation mechanisms in laser powder bed fusion additive manufacturing process. *Addit. Manuf.* **2020**, *36*, 101438. [CrossRef]
14. Boschetto, A.; Bottini, L.; Veniali, F. Roughness modeling of AlSi10Mg parts fabricated by selective laser melting. *J. Mater. Process. Technol.* **2017**, *241*, 154–163. [CrossRef]
15. Yang, T.; Liu, T.; Liao, W.; MacDonald, E.; Wei, H.; Zhang, C.; Chen, X.; Zhang, K. Laser powder bed fusion of AlSi10Mg: Influence of energy intensities on spatter and porosity evolution, microstructure and mechanical properties. *J. Alloys Compd.* **2020**, *849*, 156300. [CrossRef]
16. Ali, U.; Esmaeilizadeh, R.; Ahmed, F.; Sarker, D.; Muhammad, W.; Keshavarzkermani, A.; Mahmoodkhani, Y.; Marzbanrad, E.; Toyserkani, E. Identification and characterization of spatter particles and their effect on surface roughness, density and mechanical response of 17-4 PH stainless steel laser powder-bed fusion parts. *Mater. Sci. Eng. A* **2019**, *756*, 98–107. [CrossRef]
17. Kazantseva, N.; Krakhmalev, P.; Yadroitsev, I.; Fefelov, A.; Merkushev, A.; Ilyinikh, M.; Vinogradova, N.; Ezhov, I.; Kurennykh, T. Oxygen and nitrogen concentrations in the Ti-6Al-4V alloy manufactured by direct metal laser sintering (DMLS) process. *Mater. Lett.* **2017**, *209*, 311–314. [CrossRef]
18. Rousseau, J.N.; Bois-Brochu, A.; Blais, C. Effect of oxygen content in new and reused powder on microstructural and mechanical properties of Ti6Al4V parts produced by directed energy deposition. *Addit. Manuf.* **2018**, *23*, 197–205. [CrossRef]
19. Denti, L.; Sola, A.; Defanti, S.; Sciancalepore, C.; Bondioli, F. Effect of Powder Recycling in Laser-based Powder Bed Fusion of Ti-6Al-4V. *Manuf. Technol.* **2019**, *19*, 190–196. [CrossRef]
20. Carrion, P.E.; Soltani-Tehrani, A.; Phan, N.; Shamsaei, N. Powder Recycling Effects on the Tensile and Fatigue Behavior of Additively Manufactured Ti-6Al-4V Parts. *JOM* **2019**, *71*, 963–973. [CrossRef]
21. Wang, M.; Zhou, J.; Yin, Y.; Nan, H.; Xue, P.; Tu, Z. Hot deformation behavior of the Ti6Al4V alloy prepared by powder hot isostatic pressing. *J. Alloys Compd.* **2017**, *721*, 320–332. [CrossRef]
22. Gasper, A.; Szost, B.; Wang, X.; Johns, D.; Sharma, S.; Clare, A.; Ashcroft, I. Spatter and oxide formation in laser powder bed fusion of Inconel 718. *Addit. Manuf.* **2018**, *24*, 446–456. [CrossRef]
23. Simonelli, M.; Tuck, C.; Aboulkhair, N.T.; Maskery, I.; Ashcroft, I.; Wildman, R.D.; Hague, R.J. A Study on the Laser Spatter and the Oxidation Reactions during Selective Laser Melting of 316L Stainless Steel, Al-Si10-Mg, and Ti-6Al-4V. *Met. Mater. Trans. A* **2015**, *46*, 3842–3851. [CrossRef]
24. Liu, S.; Shin, Y.C. Additive manufacturing of Ti6Al4V alloy: A review. *Mater. Des.* **2019**, *164*, 107552. [CrossRef]
25. Heiden, M.J.; Deibler, L.A.; Rodelas, J.M.; Koepke, J.R.; Tung, D.J.; Saiz, D.J.; Jared, B.H. Evolution of 316L stainless steel feedstock due to laser powder bed fusion process. *Addit. Manuf.* **2019**, *25*, 84–103. [CrossRef]

26. Nassar, A.R.; Gundermann, M.A.; Reutzel, E.W.; Guerrier, P.; Krane, M.H.; Weldon, M.J. Formation processes for large ejecta and interactions with melt pool formation in powder bed fusion additive manufacturing. *Sci. Rep.* **2019**, *9*, 5038. [CrossRef] [PubMed]
27. Hao, T.W.; Wong, W.L.E.; Dalgarno, K.W. An overview of powder granulometry on feedstock and part performance in the selective laser melting process. *Addit. Manuf.* **2017**, *18*, 228–255. [CrossRef]